ARTICLE IN PRESS

International Journal of Engineering Science xxx (2009) xxx–xxx

Contents lists available at ScienceDirect

International Journal of Engineering Science

journal homepage: www.elsevier.com/locate/ijengsci

Size effects in the bending of thin foils

M.I. Idiart [a,c], V.S. Deshpande [a], N.A. Fleck [a], J.R. Willis [b,*]

[a] Centre for Micromechanics, Department of Engineering, University of Cambridge, Trumpington Street, Cambridge CB2 1PZ, UK
[b] Centre for Mathematical Sciences, Department of Applied Mathematics and Theoretical Physics, University of Cambridge, Wilberforce Road, Cambridge CB3 0AL, UK
[c] Área Departamental Aeronáutica, Facultad de Ingeniería, Universidad Nacional de La Plata, Calle 1 y 47, La Plata B1900TAG, Argentina

ARTICLE INFO

Article history:
Available online xxxx

Dedicated with respect and affection to the memory of A.J.M. Spencer FRS.

Keywords:
Strain gradient plasticity
Size effects
Thin foils
Metallic foams

ABSTRACT

The plastic response of a thin foil under bending is analysed using the phenomenological flow theory of strain gradient plasticity proposed by Fleck and Willis [N.A. Fleck, J.R. Willis, A mathematical basis for strain gradient plasticity theory. Part I: scalar plastic multiplier, J. Mech. Phys. Solids 57 (2009) 161–177; N.A. Fleck, J.R. Willis, A mathematical basis for strain gradient plasticity theory. Part II: tensorial plastic multiplier, J. Mech. Phys. Solids 57 (2009) 1045–1057]. Both the scalar and the tensorial versions of the theory are considered. Numerical results for elasto-plastic and elasto-viscoplastic foils are obtained via minimum principles, and closed-form expressions are derived in the limit of vanishing elasticity. An elevation of both bending moment at yield and hardening rate is predicted with decreasing foil thickness. Predictions are in line with existing experimental data on nickel foils with inferred material length-scales in the range 1–12 μm. Finally, the theory is used to assess size effects on the strength of metallic foams.

1. Introduction

The microbending of thin foils is a fundamental materials test to underpin strain gradient plasticity theories [3–5,23,19,24]. In this test, a metallic foil of thickness in the range 10–150 μm is bent over a circular cylindrical bar whose diameter sets the value of applied curvature. The bending moment is deduced from the degree of elastic spring-back upon release of the foil from the mandrel. The bending test is a complementary test method to the wire torsion test of [10]. In both tests, the strain field varies linearly with position. However, there are useful differences:

(i) The level of imposed strain is of similar order of magnitude to the yield strain in the bend test; in contrast, the strain level at the surface of a wire in torsion is much larger, of the order of unity. This difference allows for a probing of size effects over a wide range of strain levels.
(ii) The bending moment in a foil of rectangular cross-section scales with the square of its thickness. In contrast, the torque on a wire scales with the cube of its diameter, with concomitant difficulty in measuring the torque at small twist.

Phenomenological strain gradient theories of isotropic plasticity represent a relatively simple engineering approach to modelling size effects in polycrystalline metals with leading dimensions in the range 1–100 μm. A classification of the various phenomenological strain gradient plasticity approaches proposed to date has been given by Gudmundson [13], and a

* Corresponding author.
E-mail addresses: mii23@cam.ac.uk (M.I. Idiart), vsd@eng.cam.ac.uk (V.S. Deshpande), naf1@cam.ac.uk (N.A. Fleck), J.R.Willis@damtp.cam.ac.uk (J.R. Willis).

0020-7225/$ - see front matter © 2009 Elsevier Ltd. All rights reserved.
doi:10.1016/j.ijengsci.2009.06.002

discussion on their regimes of validity can be found in [10,16]. More sophisticated approaches have been applied to the microbending of single crystals: molecular dynamics (e.g., [25]), discrete dislocation simulations (e.g., [2]), and continuum statistical dislocation theories (e.g., [26,22,27]). These sophisticated theories require extensive calibration at the dislocation level, and are not yet developed to the point where the stress versus strain response of a polycrystal can be predicted. Practical engineering alloys are multi-phase polycrystals, and there remains a need to understand size effects at the phenomenological level using a top-down approach, see for example [17]. In this paper, the microbending of thin foils is analysed using the strain gradient plasticity framework recently proposed by Fleck and Willis [8,9]. This incremental theory, which draws upon earlier work by Fleck and Hutchinson [7] and Gudmundson [13], assumes associated plastic flow and possesses a convex yield surface. Consequently, positive dissipation is ensured, and uniqueness and extremum principles can be stated.

The tensorial version of the theory is first summarised in Section 2. In Section 3, constitutive models for elasto-plastic and elasto-viscoplastic solids are described and associated minimum principles are stated. The analysis of a thin foil under bending is then carried out in Section 4, and a selection of numerical and analytical predictions is given in Section 5. Comparisons with corresponding predictions resulting from the simplified scalar framework of [8] are given in Section 6, and their implications are discussed. Finally, the results for thin foils are also used to assess the effect of cell size on the yield strength of open-cell metallic foams whose collapse is mainly due to the plastic bending of ligaments [12]. Numerical aspects of the minimization and time integration procedures utilised are described in an Appendix A.

2. Strain gradient plasticity framework

The strain gradient plasticity theory proposed by Fleck and Willis [9] makes use of the framework introduced in [13]. We summarise the main results here. In this framework, the relevant kinematical variables are the velocity $\dot{u}_i$, the elastic strain rate $\dot{\varepsilon}^{EL}_{ij}$, and the plastic strain rate $\dot{\varepsilon}^{PL}_{ij}$, which satisfy the standard kinematical relations

$$\dot{\varepsilon}_{ij} = \frac{1}{2}\left(\dot{u}_{i,j} + \dot{u}_{j,i}\right), \quad \dot{\varepsilon}_{ij} = \dot{\varepsilon}^{EL}_{ij} + \dot{\varepsilon}^{PL}_{ij}, \quad \dot{\varepsilon}^{PL}_{ii} = 0. \tag{1}$$

Both $\dot{\varepsilon}^{PL}_{ij}$ and its spatial gradient $\dot{\varepsilon}^{PL}_{ij,k}$ contribute to the internal plastic work, so that the virtual work statement reads

$$\int_V \left[\sigma_{ij}\dot{\varepsilon}^{EL}_{ij} + q_{ij}\dot{\varepsilon}^{PL}_{ij} + \tau_{ijk}\dot{\varepsilon}^{PL}_{ij,k}\right] dV = \int_S \left[T_i\dot{u}_i + t_{ij}\dot{\varepsilon}^{PL}_{ij}\right] dS \tag{2}$$

thereby defining work-conjugate stress quantities σ_{ij}, q_{ij} and τ_{ijk} in the domain V occupied by the solid, and the surface tractions T_i and t_{ij} on the external boundary S of the solid. Balance laws for the stress quantities follow directly from the principle of virtual work:

$$\sigma_{ij,j} = 0 \quad \text{and} \quad q_{ij} - \tau_{ijk,k} = \sigma'_{ij} \quad \text{in } V, \tag{3}$$

$$\sigma_{ij}n_j = T_i \quad \text{and} \quad \tau_{ijk}n_k = t_{ij} \quad \text{on } S \tag{4}$$

and $\sigma_{ij} = \sigma_{ji}, q_{ij} = q_{ji}, q_{ii} = 0, \tau_{ijk} = \tau_{jik}, \tau_{iik} = 0$. In these expressions, σ'_{ij} is the deviatoric Cauchy stress, and the normal n_i is directed outwards.

The set of equations is closed by constitutive laws relating the kinematical and work-conjugate variables appearing in the work statement (2). Specific constitutive laws for elasto-plastic and elasto-viscoplastic solids are given in the next section.

3. Constitutive models and minimum principles

Fleck and Willis [9] have proposed elasto-plastic and elasto-viscoplastic constitutive models that account for internal energy storage due to elastic straining, and for dissipation due to plastic straining and its spatial gradient. We restrict attention to *isotropic* solids.

The elastic behaviour is characterised by

$$\sigma_{ij} = \frac{\partial U}{\partial \varepsilon^{EL}_{ij}}(\varepsilon^{EL}_{ij}) = L_{ijkl}\varepsilon^{EL}_{ij} = L_{ijkl}\left(\varepsilon_{ij} - \varepsilon^{PL}_{ij}\right), \tag{5}$$

where U is the internal energy density of the solid and L_{ijkl} is a positive-definite isotropic tensor of elastic moduli.

The inelastic behaviour is characterised in terms of $\dot{\varepsilon}^{PL}_{ij}$ and its spatial gradient $\dot{\varepsilon}^{PL}_{ij,k}$. As a result, material length-scales enter naturally on dimensional grounds. In this work, we restrict attention to the simplest models, containing a single material length-scale ℓ. The notation is simplified by introducing the 20-dimensional stress and strain-rate vectors

$$\mathscr{S}_I = \left(q_{ij}, \ell^{-1}\tau_{ijk}\right), \quad \dot{\mathscr{E}}_I = \left(\dot{\varepsilon}^{PL}_{ij}, \ell\dot{\varepsilon}^{PL}_{ij,k}\right), \quad I = 1, \ldots, 20 \tag{6}$$

and by adopting the convention that a repeated subscript I denotes summation over the corresponding lower-case indices. Also, introduce the magnitudes

$$\Sigma^2 = \frac{3}{2}\mathscr{S}_I\mathscr{S}_I = \frac{3}{2}\left(q_{ij}q_{ij} + \ell^{-2}\tau_{ijk}\tau_{ijk}\right), \quad \dot{E}^2_P = \frac{2}{3}\dot{\mathscr{E}}_I\dot{\mathscr{E}}_I = \frac{2}{3}\left(\dot{\varepsilon}^{PL}_{ij}\dot{\varepsilon}^{PL}_{ij} + \ell^2\dot{\varepsilon}^{PL}_{ij,k}\dot{\varepsilon}^{PL}_{ij,k}\right). \tag{7}$$

Please cite this article in press as: M.I. Idiart et al., Size effects in the bending of thin foils, Int. J. Eng. Sci. (2009), doi:10.1016/j.ijengsci.2009.06.002

The rate of plastic dissipation is given by $\dot{D} = \mathscr{S}_I \dot{\mathscr{E}}_I = q_{ij}\dot{\varepsilon}^{PL}_{ij} + \tau_{ijk}\dot{\varepsilon}^{PL}_{ij,k}$. The second law of thermodynamics requires that $\dot{D}$ be non-negative and thereby imposes restrictions on constitutive models (see, for instance, Gudmundson [13] and Gurtin [14]). Specific models that satisfy this requirement are spelled out next.

3.1. Elasto-plastic solids

As in the case of conventional elasto-plastic solids, the elastic domain is delimited by a convex yield surface f. Note, however, that this surface is not defined in the space of deviatoric Cauchy stress tensors σ'_{ij}, but rather in the space of generalised stress vectors $\mathscr{S}_I$. The proposed yield criterion is

$$f(\mathscr{S}_I; E_P) = \Sigma - \sigma_y(E_P) = 0, \tag{8}$$

where $\sigma_y(E_P)$ is the uniaxial flow strength of the material, evaluated at the accumulated effective plastic strain $E_P = \int \dot{E}_P dt$. The strength is thus elevated by the presence of plastic strain gradients.

In order to guarantee positive dissipation, associative plastic flow is assumed, whereby

$$\dot{\mathscr{E}}_I = \begin{cases} \dfrac{3}{2}\dfrac{\dot{\Sigma}}{h(E_P)}\dfrac{\mathscr{S}_I}{\Sigma}, & \text{if } \Sigma = \sigma_y(E_P) \text{ and } \dot{\Sigma} > 0, \\ 0, & \text{otherwise.} \end{cases} \tag{9}$$

Here, $h(E_P) = \sigma'_y(E_P)$ is the hardening rate of the material and $\dot{\Sigma} = \dot{\mathscr{S}}_I \mathscr{S}_I / \Sigma$ is the projection of the generalised stress rate on the yield surface normal. During plastic loading, $\dot{\Sigma} > 0$ and continued yield implies the consistency relation $\dot{\Sigma} = h(E_P)\dot{E}_P$. The dissipation rate is thus $\mathscr{S}_I \dot{\mathscr{E}}_I = \sigma_y(E_P)\dot{E}_P \geqslant 0$, as required by thermodynamics. Non-hardening solids such that $h(E_P) = 0$ require special treatment which is not pursued further here.

The incremental boundary-value problem for the velocity $\dot{u}_i$ and plastic strain rate $\dot{\varepsilon}^{PL}_{ij}$ fields consists of the compatibility equations (1), the rate forms of the equilibrium equations (3) and (4) and of the elastic constitutive law (5), the plastic constitutive law (9), and the boundary conditions on S. Uniqueness theorems for the solution $(\dot{u}_i, \dot{\varepsilon}^{PL}_{ij})$ have been given by Fleck and Willis [9]. However, the stress vector $\mathscr{S}_I$ is uniquely determined only in the regions undergoing active plastic straining. In regions where the solid is behaving in an elastic manner, $\mathscr{S}_I$ is indeterminate but must still satisfy the balance law $(3)_2$. This is mathematically analogous to the state of stress in a conventional rigid-plastic solid (see, for example, Hill [15]).

The incremental problem can be recast in the form of two kinematical minimum principles, see [9] for the proof.

Minimum principle I. Assume the current state of stress σ_{ij} and of plastic deformation $(\varepsilon^{PL}_{ij}, E_P)$ are known everywhere in V. Let $\dot{\varepsilon}^{PL0}_{ij}$ be the prescribed plastic strain rate on the part S_U of S, and let t^0_{ij} be the prescribed traction t_{ij} on the remainder S_T. The actual distribution of plastic strain rate $\dot{\varepsilon}^{PL}_{ij}$ satisfies the minimum statement

$$\int_{S_U} t_{ij}\dot{\varepsilon}^{PL0}_{ij}\, dS = \min_{\dot{\varepsilon}^{PL}_{ij}} \left\{ \int_V \left[\sigma_y(E_P)\dot{E}_P - \sigma'_{ij}\dot{\varepsilon}^{PL}_{ij}\right] dV - \int_{S_T} t^0_{ij}\dot{\varepsilon}^{PL}_{ij}\, dS \right\}, \tag{10}$$

where the minimum is taken over fields $\dot{\varepsilon}^{PL}_{ij}$ such that $\dot{\varepsilon}^{PL}_{ij} = \dot{\varepsilon}^{PL0}_{ij}$ on S_U. The minimum value of the functional gives the external plastic work rate expended on S_U. This principle is a close analogue to the upper bound theorem of [15] for standard rigid-plastic solids.

The part of V where $\dot{\varepsilon}_P > 0$ constitutes the active plastic region V_P. In general, V_P is a set of disjoint zones V_{P_α}. If a non-zero value of $\dot{\varepsilon}^{PL}_{ij}$ is prescribed somewhere on the boundary of a given zone, the minimum principle (10) delivers the unique plastic strain-rate distribution within that zone. Otherwise, the minimum principle (10) delivers $\dot{\varepsilon}^{PL}_{ij}$ within the zone up to a multiplicative constant, since the relevant functional is homogeneous of degree one in $\dot{\varepsilon}^{PL}_{ij}$. In that case, it is convenient to set $\dot{\varepsilon}^{PL}_{ij} = \dot{\lambda}_\alpha \hat{\varepsilon}^{PL}_{ij}$, where $\dot{\lambda}_\alpha$ is a uniform plastic multiplier and $\hat{\varepsilon}^{PL}_{ij}$ is a plastic strain-rate distribution of unit 'magnitude',

$$\frac{1}{V_{P_\alpha}} \int_{V_{P_\alpha}} \hat{\varepsilon}^{PL}_{ij}\hat{\varepsilon}^{PL}_{ij} dV = 1. \tag{11}$$

The minimum principle (10) then delivers the unique distribution $\hat{\varepsilon}^{PL}_{ij}$ within the zone V_{P_α}, but the plastic multiplier $\dot{\lambda}_\alpha$ must be determined from a second minimum principle, together with the velocity field $\dot{u}_i$.

Minimum principle II. Let $\dot{u}^0_i$ be the prescribed velocity on S_U, and let $\dot{T}^0$ and $\dot{t}^0_{ij}$ be the prescribed traction rates on S_T. The actual velocity field $\dot{u}_i$ and plastic multipliers $\dot{\lambda}_\alpha$, consistent with the plastic strain rate distribution obtained in (10), satisfy the minimum statement

$$\Psi = \min_{\dot{u}_i, \dot{\lambda}_\alpha} \left\{ \int_V \frac{1}{2}\left[\left(\dot{\varepsilon}_{ij} - \dot{\varepsilon}^{PL}_{ij}\right) L_{ijkl}\left(\dot{\varepsilon}_{kl} - \dot{\varepsilon}^{PL}_{kl}\right) + h(E_P)\dot{E}^2_P\right] dV - \int_{S_T} \left[\dot{T}^0_i \dot{u}_i + \dot{t}^0_{ij}\dot{\varepsilon}^{PL}_{ij}\right] dS \right\}, \tag{12}$$

where the minimum is taken over uniform $\dot{\lambda}_\alpha \geqslant 0$ and continuous fields $\dot{u}_i$ such that $\dot{u}_i = \dot{u}^0_i$ on S_U. In the absence of strain gradient effects, statement (10) is trivially satisfied, and (12) reduces to the minimum principle of [18] for standard elasto-plastic solids, which delivers the complete solution to the incremental boundary-value problem.

Please cite this article in press as: M.I. Idiart et al., Size effects in the bending of thin foils, Int. J. Eng. Sci. (2009), doi:10.1016/j.ijengsci.2009.06.002

3.2. Elasto-viscoplastic solids

Systematic experimental studies are missing for size effects in the creep regime. Geometrically necessary dislocations with attendant strengthening are still expected to play a role in the creep regime, giving a physical basis for strain gradient viscoplastic models. The proposed model consists of a non-negative, convex dissipation potential $\phi(\dot{E}_P)$ such that

$$\mathscr{S}_I = \frac{2}{3}\phi'(\dot{E}_P)\frac{\dot{\mathscr{E}}_I}{\dot{E}_P}. \tag{13}$$

The potential ϕ could also be made to depend on E^p. Noting that $\Sigma = \phi'(\dot{E}_P)$, the dissipation rate is $\dot{D} = \Sigma\dot{E}_P \geqslant 0$, as demanded by thermodynamics. Also, it is worth noting that, unlike the above elasto-plastic model, this model does not involve an elastic domain. Consequently, the stress vector $\mathscr{S}_I$ is uniquely determined everywhere in V. For this reason, rate-dependent models of this type are often employed with low strain-rate sensitivities to approximate rate-independent models of the type given in Section 3.1 (e.g., [1,11]).

As in the case of elasto-plastic solids, the incremental boundary-value problem can be cast in the form of two kinematical minimum principles.

Minimum principle I. Assume the current state of stress σ_{ij} and of plastic deformation ε^{PL}_{ij} is known everywhere in V. Let $\dot{\varepsilon}^0_P$ be the prescribed plastic strain rate on the part S_U of S, and let t^0_{ij} be the prescribed traction t_{ij} on the remainder S_T. The actual distribution of plastic strain rate $\dot{\varepsilon}^{PL}_{ij}$ satisfies the minimum statement

$$\int_{S_U} t_{ij}\dot{\varepsilon}^{PL0}_{ij}\,dS = \min_{\dot{\varepsilon}^{PL}_{ij}}\left\{\int_V\left[\phi(\dot{E}_P) - \sigma'_{ij}\dot{\varepsilon}^{PL}_{ij}\right]dV - \int_{S_T} t^0_{ij}\dot{\varepsilon}^{PL}_{ij}dS\right\}, \tag{14}$$

where the minimum is taken over fields $\dot{\varepsilon}^{PL}_{ij}$ such that $\dot{\varepsilon}^{PL}_{ij} = \dot{\varepsilon}^{PL0}_{ij}$ on S_U.

Minimum principle II. Let $\dot{u}^0_i$ be the prescribed velocity on S_U, and let $\dot{T}^0_i$ be the prescribed traction rate on S_T. The actual velocity field $\dot{u}_i$, consistent with the plastic strain rate distribution obtained in (14), satisfies the minimum statement

$$\Psi = \min_{\dot{u}_i}\left\{\frac{1}{2}\int_V\left(\dot{\varepsilon}_{ij} - \dot{\varepsilon}^{PL}_{ij}\right)L_{ijkl}\left(\dot{\varepsilon}_{kl} - \dot{\varepsilon}^{PL}_{kl}\right)dV - \int_{S_T}\dot{T}^0_i\dot{u}_i dS\right\}, \tag{15}$$

where the minimum is taken over continuous fields $\dot{u}_i$ such that $\dot{u}_i = \dot{u}^0_i$ on S_U, and $\dot{\varepsilon}^{PL}_{ij}$ is the solution to (14).

4. Analysis of a thin foil under bending

The constitutive models described in the previous section are used here to analyse a foil of thickness $2H$ subjected to pure bending. The coordinate system shown in Fig. 1 is employed throughout. Following Stölken and Evans [24], it is assumed that curvature is imposed via displacement boundary conditions at the ends of the foil, and traction-free boundary conditions are imposed on the top and bottom surfaces of the foil: $T^0_i = t^0_{ij} = 0$ at $x_2 = \pm H$. Plane strain conditions are invoked, and material incompressibility is assumed for simplicity. The analysis is restricted to the upper half of the foil $0 \leqslant x_2 \leqslant H$; the fields in the lower half follow immediately from symmetry considerations.

The total strain-rate tensor is given by

$$\dot{\varepsilon}_{11} = -\dot{\varepsilon}_{22} = \dot{\kappa}x_2, \quad \dot{\varepsilon}_{12} = 0, \quad \dot{\varepsilon}_{i3} = 0 \tag{16}$$

in terms of the rate of curvature $\dot{\kappa}$. In turn, the plastic strain rate tensor can be expressed in terms of a single scalar function $\dot{\varepsilon}_P(x_2)$, which can be positive or negative, such that

$$\dot{\varepsilon}^{PL}_{11} = -\dot{\varepsilon}^{PL}_{22} = \frac{\sqrt{3}}{2}\dot{\varepsilon}_P(x_2), \quad \dot{\varepsilon}^{PL}_{12} = 0, \quad \dot{\varepsilon}^{PL}_{i3} = 0. \tag{17}$$

In turn, the effective plastic strain rate (7) takes the form

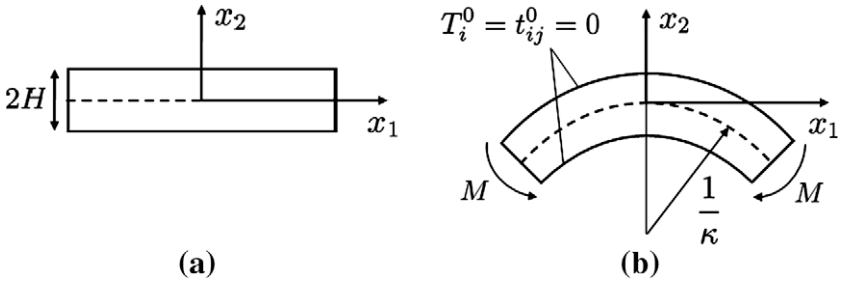

Fig. 1. Side view of foil: (a) undeformed and (b) deformed.

Please cite this article in press as: M.I. Idiart et al., Size effects in the bending of thin foils, Int. J. Eng. Sci. (2009), doi:10.1016/j.ijengsci.2009.06.002

$$\dot{E}_P = \sqrt{\dot{\varepsilon}_P^2 + \left(\ell\dot{\varepsilon}_P'\right)^2}, \tag{18}$$

where $(\cdot)' \equiv d(\cdot)/dx_2$. Finally, the equilibrium condition $(3)_1$ together with the traction-free boundary conditions and the elastic constitutive law (5) require the Cauchy stress tensor to be

$$\sigma_{11} = \frac{4}{3}E(\varepsilon_{11} - \varepsilon_{11}^{PL}), \quad \sigma_{22} = \sigma_{12} = 0, \quad \sigma_{33} = \frac{\sigma_{11}}{2}, \tag{19}$$

where E denotes the material Young's modulus.

The plastic strain rate distribution $\dot{\varepsilon}_P(x_2)$ is obtained below for elasto-plastic and elasto-viscoplastic foils by means of the minimum principles stated in Section 3. Symmetry dictates that $\dot{\varepsilon}_P(x_2)$ is an odd function, and so the analysis can be restricted to the upper half of the foil, with the additional boundary condition $\dot{\varepsilon}_P(0) = 0$.

The bending moment M is defined as the work-conjugate of the curvature κ, so that the external work rate is $M\dot{\kappa}$. The work statement (2) implies that

$$M\dot{\kappa} = 2\int_0^H \left[\sigma_{11}\dot{\varepsilon}_{11}^{EL} + 2q_{11}\dot{\varepsilon}_{11}^{PL} + 2\tau_{112}\dot{\varepsilon}_{11,2}^{PL}\right]dx_2 = 2\int_0^H \sigma_{11}\dot{\varepsilon}_{11}\,dx_2 + 4\tau_{112}\dot{\varepsilon}_{11}^{PL}\big|_{x_2=H} \tag{20}$$

and in view of (16) we obtain

$$M = 2\int_0^H \sigma_{11}x_2\,dx_2 + 2\sqrt{3}\tau_{112}\frac{\dot{\varepsilon}_P}{\dot{\kappa}}\bigg|_{x_2=H}. \tag{21}$$

As already pointed out by Engelen et al. [4], the first term in this expression is the standard contribution of axial stresses, but the second term is a non-standard contribution of higher-order tractions. In the presence of elasticity, the second term vanishes in view of the boundary condition $t_{ij} = 0$ at $x_2 = H$, and the standard expression for the bending moment is recovered. In the limit of vanishing elasticity (i.e., $E \to \infty$), however, the solution demands τ_{112} to have a finite value at the top/bottom surfaces of the foil (see below).

4.1. Elasto-plastic foils

We consider a material with uniaxial tensile stress–strain curve characterised by a Ramberg–Osgood law

$$\frac{\varepsilon}{\varepsilon_0} = \frac{\sigma}{\sigma_0} + \left(\frac{\sigma}{\sigma_0}\right)^n, \tag{22}$$

where $\varepsilon_0 = \sigma_0/E, \sigma_0$ is a flow stress, and $n = 1/N$ is a hardening exponent. For this choice, the strength of the solid is $\sigma_y(E_P) = \sigma_0(E_P/\varepsilon_0)^N$ and the hardening rate is $h(E_P) = NE(E_P/\varepsilon_0)^{N-1}$. Upon loading, plasticity develops from the outset throughout the specimen, so that no elastic–plastic boundary is present.

The plastic strain rate distribution $\dot{\varepsilon}_P(x_2)$ follows from the two minimum principles of Section 3.1. For the boundary conditions considered here, minimum principle (10) delivers $\dot{\varepsilon}_P(x_2)$ up to a multiplicative constant. We thus set $\dot{\varepsilon}_P(x_2) = \dot{\lambda}\hat{\varepsilon}_P(x_2)$, and determine $\hat{\varepsilon}_P(x_2)$ from

$$I = \min_{\hat{\varepsilon}_P}\int_0^H \left[\sigma_y(E_P)\widehat{E}_P - \frac{\sqrt{3}}{2}\sigma_{11}\hat{\varepsilon}_P\right]dx_2, \tag{23}$$

where $\widehat{E}_P = \sqrt{\hat{\varepsilon}_P^2 + (\ell\hat{\varepsilon}_P')^2}$, and the minimum is taken over fields $\hat{\varepsilon}_P(x_2)$ such that $\hat{\varepsilon}_P(0) = 0$ and $(1/H)\int_0^H \hat{\varepsilon}_P^2\,dx_2 = 1$. The multiplier $\dot{\lambda}$ then follows from minimum principle (12),

$$\Psi = \min_{\dot{\lambda}}\int_0^H \left[E\left(\frac{2}{\sqrt{3}}\dot{\kappa}x_2 - \dot{\lambda}\hat{\varepsilon}_P\right)^2 + h(E_P)\dot{\lambda}^2\widehat{E}_P^2\right]dx_2, \tag{24}$$

where the minimum is taken over $\dot{\lambda} \geqslant 0$. The minimization in (24) is straightforward, giving

$$\dot{\lambda} = \frac{2}{\sqrt{3}}E\dot{\kappa}\frac{\int_0^H \hat{\varepsilon}_P x_2\,dx_2}{\int_0^H \left(E\hat{\varepsilon}_P^2 + h(E_P)\widehat{E}_P^2\right)dx_2} \tag{25}$$

or zero if the right-hand side is negative.

The plastic strain rate $\hat{\varepsilon}_P(x_2)$ is obtained by finite element discretization of the functional in (23) and subsequent minimization with respect to the nodal amplitudes, while time integration of the rates is performed by means of a forward-Euler scheme. Details of the numerical implementation are given in Appendix A.

4.2. Elasto-viscoplastic foils

We consider solids undergoing power-law creep, characterised by

Please cite this article in press as: M.I. Idiart et al., Size effects in the bending of thin foils, Int. J. Eng. Sci. (2009), doi:10.1016/j.ijengsci.2009.06.002

$$\phi(\dot{E}_P) = \frac{\sigma_0 \dot{\varepsilon}_0}{1+m}\left(\frac{\dot{E}_P}{\dot{\varepsilon}_0}\right)^{1+m}, \tag{26}$$

where σ_0 is a flow stress, $\dot{\varepsilon}_0$ is a reference strain rate, and m is the strain-rate sensitivity, such that $0 \leqslant m \leqslant 1$. This is a generalisation of the standard power-law model, commonly used to characterise high temperature creep in metals.

The plastic strain rate distribution in the foil follows from minimum principle (14), which takes the form

$$I = \min_{\dot{\varepsilon}_P} \int_0^H \left[\frac{\sigma_0 \dot{\varepsilon}_0}{1+m}\left(\frac{\dot{E}_P}{\dot{\varepsilon}_0}\right)^{1+m} - \frac{\sqrt{3}}{2}\sigma_{11}\dot{\varepsilon}_P\right] dx_2 \tag{27}$$

subject to $\dot{\varepsilon}_P(0) = 0$. The minimum principle (15) is not required here because the total strain rate (16) is kinematically determined. Numerical minimization and time integration is carried out following a similar strategy to that outlined in Appendix A for elasto-plastic solids.

5. Results and discussion

5.1. Elasto-plastic foils

In this section we explore the dependence of bending response on the ratio of material length-scale ℓ to foil half-thickness H, for the choice $N = 0.1$. Fig. 2a shows plots of moment versus curvature, normalised by $M_y = (2/\sqrt{3})\sigma_0 H^2$ and $\kappa_y = (\sqrt{3}/2)\varepsilon_0/H$, respectively, for three values of ℓ/H. The case $\ell/H = 0$ corresponds to standard elasto-plastic foils with no gradient effects. The predictions show a strong size effect with increasing ratio ℓ/H, on both initial yielding and subsequent hardening rate. For example, the flow stress in the plastic range is elevated by a factor of 2.5 when ℓ/H is increased from zero to unity. This is on the order of strength elevation observed in nickel foils [24,19] and copper micro-beams [20].

Fig. 2b shows the underlying distribution of elastic and plastic axial strain, deep in the plastic range. In the absence of gradient effects ($\ell/H = 0$), the elastic strains are very small throughout the foil, and the plastic strains exhibit a linear profile as dictated by (16). In contrast, corresponding distributions in the gradient-plastic solid ($\ell/H = 1$) show a boundary layer near the top surface of the foil, where the plastic strain is reduced in order to meet the higher-order boundary condition $t^0_{ij} = 0$. To comply with the imposed bending deformation, this reduction of plastic strain in the boundary layer is compensated by higher elastic strains, which in turn lead to higher Cauchy stresses. If the Young's modulus E is increased, the boundary layer becomes thinner and the axial Cauchy stress within it increases. In the rigid-plastic limit, the axial Cauchy stress becomes a delta function at the top surface of the foil, and this gives a finite contribution to the external work, as represented by the second term in (21).

It is instructive to explore the rigid-plastic limit of material behaviour as this allows for closed-form expressions for the bending response. In this limit, plastic strain rates (17) coincide with the total strain rates (16), and so

$$\dot{E}_P = \frac{2}{\sqrt{3}}\dot{\kappa}\sqrt{x_2^2 + \ell^2}. \tag{28}$$

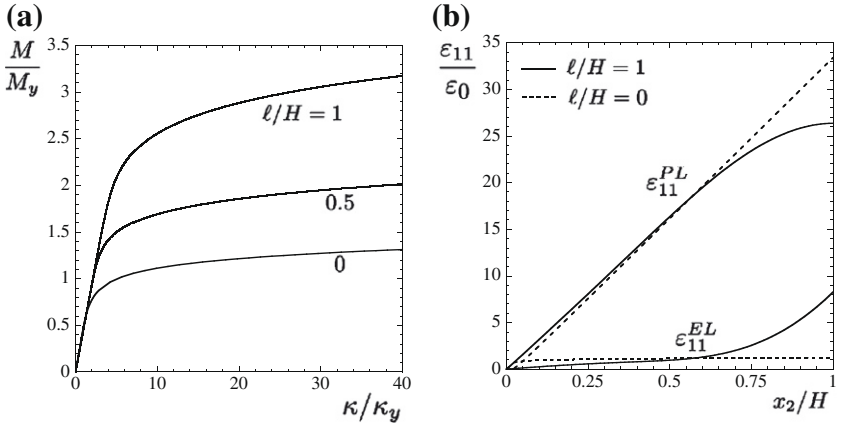

Fig. 2. Elasto-plastic foils of various ratios ℓ/H, with strain hardening exponent $N = 0.1$. (a) Normalised moment versus curvature and (b) distribution of elastic and axial plastic strain at $\kappa = 40\kappa_y$.

Please cite this article in press as: M.I. Idiart et al., Size effects in the bending of thin foils, Int. J. Eng. Sci. (2009), doi:10.1016/j.ijengsci.2009.06.002

The stress quantities then follows from (9),

$$q_{11} = \frac{2}{3}\sigma_y(E_P)\frac{\dot{\varepsilon}^{PL}_{11}}{\dot{E}_P} = \frac{1}{\sqrt{3}}\sigma_y(E_P)\frac{x_2}{\sqrt{x_2^2+\ell^2}}, \tag{29}$$

$$\tau_{112} = \frac{2}{3}\sigma_y(E_P)\frac{\ell^2\dot{\varepsilon}^{PL}_{11,2}}{\dot{E}_P} = \frac{1}{\sqrt{3}}\sigma_y(E_P)\frac{\ell^2}{\sqrt{x_2^2+\ell^2}} \tag{30}$$

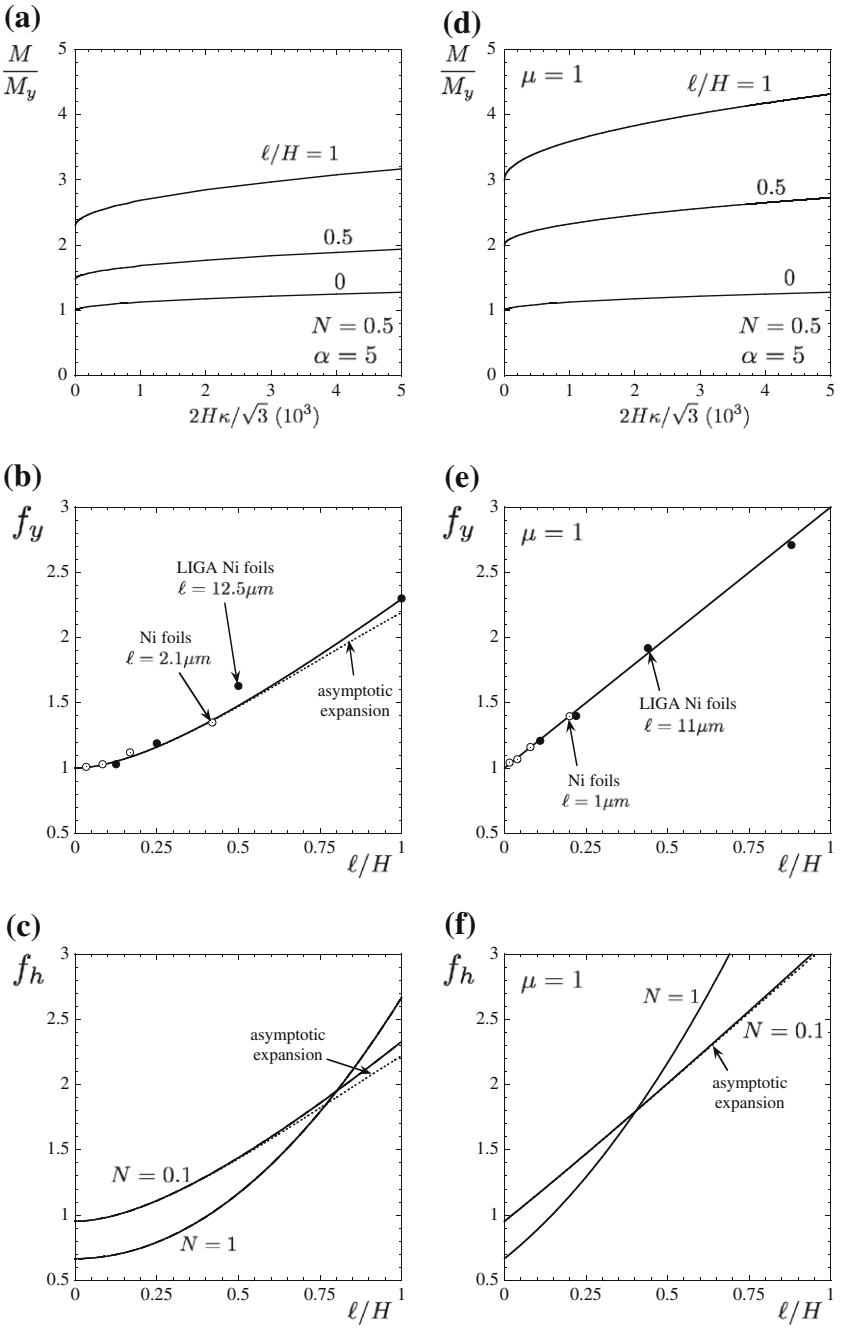

Fig. 3. Rigid-plastic foils. (a) Normalised moment versus curvature, for hardening parameters $\alpha = 5$ and $N = 0.5$; (b) normalised yield moment and (c) hardening rate as a function of ℓ/H. LIGA Ni foils data taken from [23], and Ni foils data from [19]. (d–f) Corresponding results for generalised measures with $\mu = 1$.

Please cite this article in press as: M.I. Idiart et al., Size effects in the bending of thin foils, Int. J. Eng. Sci. (2009), doi:10.1016/j.ijengsci.2009.06.002

and the Cauchy stress follows from $(3)_2$. As anticipated, τ_{112} does not vanish at $x_2 = H$, and thereby contributes to the bending moment through the non-standard term in (21). The resulting moment can be written as

$$M = \frac{4}{\sqrt{3}} \int_0^H \sigma_y(E_P) \sqrt{x_2^2 + \ell^2}\, dx_2. \tag{31}$$

For definiteness, consider a solid with the power-law hardening characteristic

$$\sigma_y(E_P) = \sigma_0 \left(1 + \alpha E_P^N\right). \tag{32}$$

For this choice, integration of (31) gives

$$\frac{M}{M_y} = f_y(\ell/H) + \alpha f_h(\ell/H, N) \left(\frac{2}{\sqrt{3}} H\kappa\right)^N, \tag{33}$$

where $M_y = (2/\sqrt{3})\sigma_0 H^2$, and

$$f_y(\beta) = \sqrt{1+\beta^2} + \beta^2 \sinh^{-1}(\beta^{-1}), \tag{34}$$

$$f_h(\beta, N) = 2\beta^{1+N}\, {}_2F_1\left(\frac{1}{2}, -\frac{1+N}{2}; \frac{3}{2}; -\frac{1}{\beta^2}\right). \tag{35}$$

In the last expression, ${}_2F_1$ denotes the standard hypergeometric series.[1] These expressions are well approximated by their simpler asymptotic expansions about $\ell/H = 0$,

$$f_y(\beta) = 1 + \beta^2 |\ln \beta| + \frac{1+\ln 4}{2}\beta^2 + O(\beta^4), \tag{36}$$

$$f_h(\beta, N) = \frac{2}{2+N} + \frac{1+N}{N}\beta^2 + \sqrt{\pi}\frac{\Gamma\left(-1-\frac{N}{2}\right)}{\Gamma\left(-\frac{1+N}{2}\right)}\beta^{2+N} + O(\beta^4), \tag{37}$$

where Γ denotes the Euler gamma function. It is noted that the expression (37) given by the first three terms agrees exactly with (35) for $N = 1$; the range of validity of (37) vanishes as $N \to 0$.

Predictions for the normalised bending moment versus curvature, as given by (33), are shown in Fig. 3a for hardening parameters $N = 0.5$ and $\alpha = 5$ as used by Evans and Hutchinson [5] to model nickel foils. Size effects are predicted for both the yield point and the hardening rate, see Fig. 3b and c.

It is instructive to compare the predictions for bending moment at yield with the recent experimental data of [19] for Ni foils and of [23] for LIGA Ni foils. Data on Ni foils was extracted from the regression lines given in Fig. 3 of [19] for bending moment at yield versus grain size, while data on LIGA Ni foils was extracted from the regression lines given in Fig. 2 of [23] for bending moment versus curvature, evaluated at a small value of bending curvature. In plotting the experimental data for each grade of foil, values of σ_0 and ℓ are chosen, independent of foil thickness, in order to give the best agreement with the predictions, see Fig. 3b. The inferred material length- scales are $\ell = 2.1$ μm for the Ni foils, and $\ell = 12.5$ μm for the LIGA Ni foils. These values lie within the expected range [7,5]. The formulae (34)–(37) thus provide a simple and versatile means of extracting material length-scales from experimental data.

We note that the strain gradient plasticity theory considered here will generally predict stronger size effects than the earlier flow theory of [7]. This is because the initial yield point in the new theory incorporates a dependence on the higher-order stresses τ_{ijk} which need not vanish in the elastic domain. In contrast, the flow theory of [7] assumes that the higher-order stresses are zero until plasticity develops. Consequently, the predicted initial yield point is independent of specimen size, as already noted by Engelen et al. [4] and Niordson [21].

An alternative plastic strain measure. The constitutive models described in Section 3 are phrased in terms of the 'overall effective' stress and plastic strain rate measures (7). Fleck and Hutchinson [6] have proposed a family of generalised measures, which in the present context take the form

$$\Sigma = \sqrt{\frac{3}{2}}\left[\left(q_{ij}q_{ij}\right)^{\frac{\mu}{2(\mu-1)}} + \left(\ell^{-2}\tau_{ijk}\tau_{ijk}\right)^{\frac{\mu}{2(\mu-1)}}\right]^{\frac{\mu-1}{\mu}}, \quad \dot{E}_P = \sqrt{\frac{2}{3}}\left[\left(\dot{\varepsilon}_{ij}^{PL}\dot{\varepsilon}_{ij}^{PL}\right)^{\frac{\mu}{2}} + \left(\ell^2 \dot{\varepsilon}_{ij,k}^{PL}\dot{\varepsilon}_{ij,k}^{PL}\right)^{\frac{\mu}{2}}\right]^{\frac{1}{\mu}}. \tag{38}$$

The exponent μ constitutes an additional material parameter. For rigid-plastic foils, the generalised plastic strain rate measure is

$$\dot{E}_P = \frac{2}{\sqrt{3}}\dot{\kappa}\left(x_2^\mu + \ell^\mu\right)^{\frac{1}{\mu}} \tag{39}$$

[1] See, for instance, M. Abramowitz, I.A. Stegun, Handbook of Mathematical Functions with Formulas, Graphs, and Mathematical Tables, Dover, New York, 1972.

Please cite this article in press as: M.I. Idiart et al., Size effects in the bending of thin foils, Int. J. Eng. Sci. (2009), doi:10.1016/j.ijengsci.2009.06.002

and the stress quantities follows from normality to the yield surface (8),

$$q_{11} = \frac{2}{3}\sigma_y(E_P)\left(\frac{\dot{\varepsilon}_P}{\dot{E}_P}\right)^{\mu-1} = \frac{1}{\sqrt{3}}\sigma_y(E_P)\frac{x_2^{\mu-1}}{\left(x_2^{\mu}+\ell^{\mu}\right)^{\frac{\mu-1}{\mu}}}, \tag{40}$$

$$\ell^{-1}\tau_{112} = \frac{2}{3}\sigma_y(E_P)\left(\frac{\ell\dot{\varepsilon}'_P}{\dot{E}_P}\right)^{\mu-1} = \frac{1}{\sqrt{3}}\sigma_y(E_P)\frac{\ell^{\mu-1}}{\left(x_2^{\mu}+\ell^{\mu}\right)^{\frac{\mu-1}{\mu}}}. \tag{41}$$

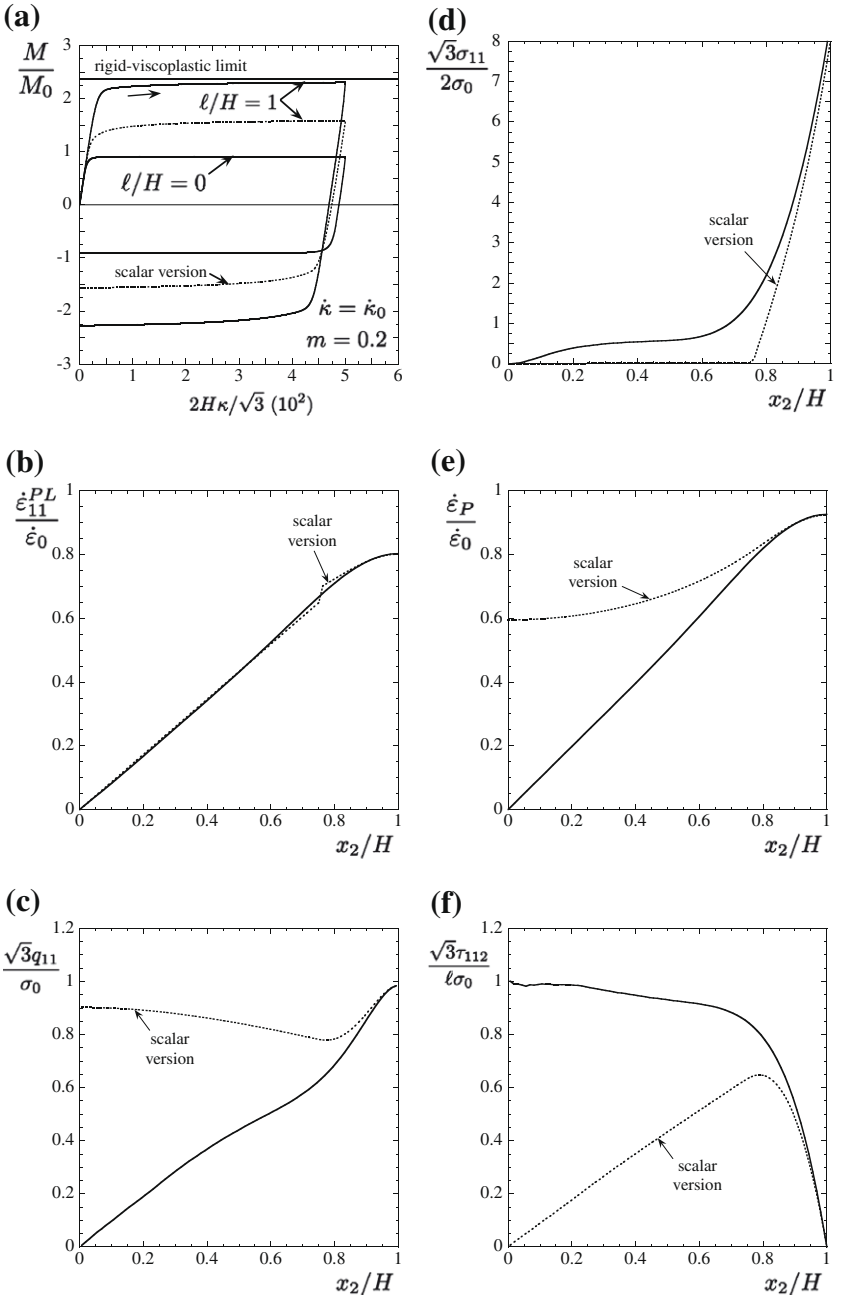

Fig. 4. Elasto-viscoplastic foils with strain-rate sensitivity $m = 0.2$ and Young's modulus $E = 1000\sigma_0$. (a) Normalised moment versus curvature and (b–f) local fields for $\ell/H = 1$ and $2H\kappa/\sqrt{3} = 0.05$. The rate of applied curvature is $\dot{\kappa} = \dot{\kappa}_0$. Throughout, solid lines and dotted lines denote the tensorial and scalar version of the theory, respectively.

Please cite this article in press as: M.I. Idiart et al., Size effects in the bending of thin foils, Int. J. Eng. Sci. (2009), doi:10.1016/j.ijengsci.2009.06.002

The Cauchy stress then follows from $(3)_2$, and the resulting moment can be written as

$$M = \frac{4}{\sqrt{3}} \int_0^H \sigma_y(E_P)\left(x_2^{\mu} + \ell^{\mu}\right)^{\frac{1}{\mu}} dx_2. \tag{42}$$

The constitutive models of Section 3 correspond to the choice $\mu = 2$. Based on dislocation arguments, Fleck and Hutchinson [6] have suggested the alternative value $\mu = 1$ (see also [5]). For this choice and power-law hardening (32), the bending moment is of the same form (33), with

$$f_y(\beta) = 1 + 2\beta, \tag{43}$$

$$f_h(\beta, N) = 2\frac{(1+\beta)^{2+N} - \beta^{2+N}}{2+N}. \tag{44}$$

The asymptotic behaviour of f_h about $\ell/H = 0$ is

$$f_h(\beta, N) = \frac{2}{2+N} + 2\beta + (1+N)\beta^2 - \frac{2}{2+N}\beta^{2+N} + O\left(\beta^3\right). \tag{45}$$

The resulting predictions are shown in Fig. 3d–f. Stronger size effects relative to those of Fig. 3a–c are observed. This is made explicit by the asymptotic behaviour for small ℓ/H of the bending moment at yield f_y and the hardening rate f_h. For $\mu = 2$, the strengthening effect in f_y and f_h scales with $(\ell/H)^2|\ln(\ell/H)|$ and $(\ell/H)^2$, respectively, see expressions (36) and (37), while for $\mu = 1$ it scales linearly with ℓ/H, see expressions (43) and (45). A similar conclusion was drawn by Fleck and Hutchinson [6]. In Fig. 3e, the predictions (43) are compared with the experimental results of [19,23] on nickel foils as already introduced. Good agreement between predictions and experimental observations is obtained if the length-scales are taken to be $\ell = 1$ μm for the nickel foils, and $\ell = 11$ μm for the LIGA nickel foils. Thus, the preliminary comparisons shown in Fig. 3b and e do not suggest a particular choice of μ. It is remarked, however, that the different trends predicted for the bending moment with $\mu = 1$ and 2 in the range of small ℓ/H do provide an opportunity to establish the choice of μ once larger sets of experimental data become available.

5.2. Elasto-viscoplastic foils

Fig. 4 explores the variation of bending response with ℓ/H, in foils with strain-rate sensitivity $m = 0.2$ and Young's modulus $E = 1000\sigma_0$. Each specimen was loaded at a rate of curvature $\dot{\kappa}_0 = (\sqrt{3}\dot{\varepsilon}_0/2H)$ until the curvature attained the value $(2H\kappa/\sqrt{3}) = 0.05$. The curvature rate was then reversed in sign and the specimen was reversed loaded until curvature attained the value zero. The predicted bending moment normalised by $M_0 = (2/\sqrt{3})\sigma_0 H^2$ is shown in Fig. 4a (solid lines[2]) as a function of curvature. In the plastic range, thin foils with thickness ratio 1 plateau at a bending moment ~ 2.5 times higher than thick foils ($\ell/H = 0$). Upon load reversal, the foils unload elastically until the moment attains the reversed peak value. No reverse plasticity develops at zero moment, in support of the common assumption made in deducing the bending moment from elastic spring-back [24]. It is noted, however, that strain gradient plasticity models can predict reverse plasticity and Bauchinger effects if the internal energy U of the solid is taken to depend on accumulated plastic strain and its gradient (see, for instance, Anand et al. [1]). Experimental characterisation of unloading and reversed loading of thin foils would provide useful insight in this regard.

Fig. 4b–f shows the underlying field distributions at $(2H\kappa/\sqrt{3}) = 0.05$. The solution for $\ell/H = 1$ is far from that for a conventional solid. It is evident from Fig. 4f that flow is activated mainly by the higher-order stresses over a domain of size $\sim \ell$. Over much of the foil, the stress quantity q_{11} is much smaller than $\ell^{-1}\tau_{112}$, and σ_{11} is below σ_0, see Fig. 4c and d. However, an elastic boundary layer develops near the top/bottom surfaces, where the Cauchy stress is several times higher than the flow stress σ_0 of the solid, see Fig. 4d. As ℓ/H goes to zero, strain gradient effects become less important and the distribution of Cauchy stress over the cross-section of the foil approaches the classical result, as expected, see Fig. 5a. Deep in the plastic range, the bending moment asymptotes that of a rigid-viscoplastic foil, derived as follows.

The kinematics of rigid-plastic foils carry over to rigid-viscoplastic foils, so that the effective plastic strain rate is given by (28), and the stress quantities follows from (26):

$$q_{11} = \frac{2}{3}\phi'(\dot{E}_P)\frac{\dot{\varepsilon}^{PL}_{11}}{\dot{E}_P} = \frac{1}{\sqrt{3}}\frac{x_2}{\left(x_2^2 + \ell^2\right)^{\frac{1-m}{2}}}\sigma_0\left(\frac{2}{\sqrt{3}}\frac{\dot{\kappa}}{\dot{\varepsilon}_0}\right)^m, \tag{46}$$

$$\tau_{112} = \frac{2}{3}\phi'(\dot{E}_P)\frac{\ell^2\dot{\varepsilon}^{PL}_{11,2}}{\dot{E}_P} = \frac{1}{\sqrt{3}}\frac{\ell^2}{\left(x_2^2 + \ell^2\right)^{\frac{1-m}{2}}}\sigma_0\left(\frac{2}{\sqrt{3}}\frac{\dot{\kappa}}{\dot{\varepsilon}_0}\right)^m. \tag{47}$$

The Cauchy stress then follows from $(3)_2$. Once again, τ_{112} does not vanish on the top/bottom surfaces of the foil, and so contributes to the bending moment through the non-standard term in (21). The resulting moment can be written as

[2] Simplified predictions resulting from a scalar version of the model (dotted lines) are discussed in Section 6.

Please cite this article in press as: M.I. Idiart et al., Size effects in the bending of thin foils, Int. J. Eng. Sci. (2009), doi:10.1016/j.ijengsci.2009.06.002

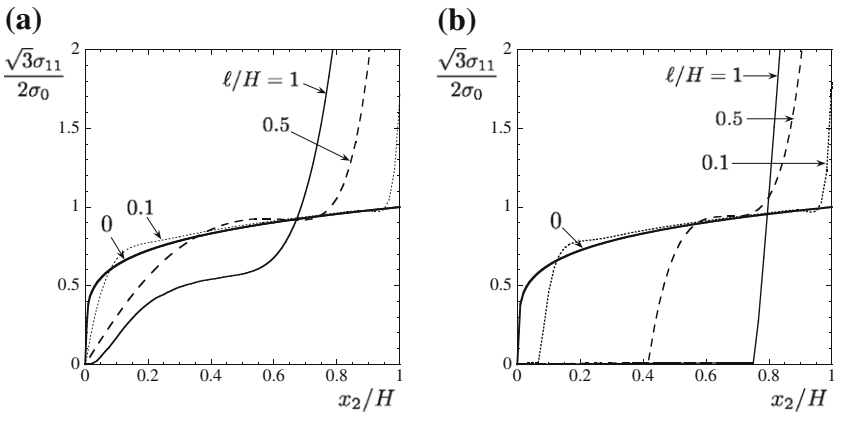

Fig. 5. Distribution of axial Cauchy stress at $2H\kappa/\sqrt{3} = 0.05$, for various thickness ratios ℓ/H: (a) tensorial theory and (b) scalar theory.

$$M = \frac{4}{\sqrt{3}}\sigma_0\left(\frac{2}{\sqrt{3}}\frac{\dot{\kappa}}{\dot{\varepsilon}_0}\right)^m \int_0^H (x_2^2 + \ell^2)^{\frac{1+m}{2}}\, dx_2. \tag{48}$$

Integration of (48) finally gives

$$\frac{M}{M_0} = f_h(\ell/H, m)\left(\frac{\dot{\kappa}}{\dot{\kappa}_0}\right)^m, \tag{49}$$

where f_h is given by (35), and the reference magnitudes M_0 and $\dot{\kappa}_0$ have been introduced above. Expression (49) gives the limiting bending moment sustained by an elasto-viscoplastic foil, see Fig. 4a. The dependence of f_h upon ℓ/H has already been given in Fig. 3c.

6. Analysis based on the simplified scalar framework

The theory outlined in Sections 2 and 3 treats the plastic strain rate *tensor* $\dot{\varepsilon}_{ij}^{PL}$ as a free kinematic quantity. Fleck and Willis [8] have proposed a simplified framework for isotropic solids, along the lines of [7], where the plastic strain rate tensor is taken to be colinear with the deviatoric Cauchy stress tensor,

$$\dot{\varepsilon}_{ij}^{PL} = \dot{\varepsilon}_P m_{ij}, \quad m_{ij} = \frac{3}{2}\frac{\sigma'_{ij}}{\sigma_e}, \tag{50}$$

$\sigma_e^2 = (3/2)\sigma'_{ij}\sigma'_{ij}$, and the *scalar* plastic multiplier $\dot{\varepsilon}_P \geqslant 0$ is the primary kinematic unknown in addition to the displacement rate $\dot{u}_i$.

Internal plastic work is expended by $\dot{\varepsilon}_P$ and its spatial gradient $\dot{\varepsilon}_{P,i}$, so that the virtual work statement reads

$$\int_V \left[\sigma_{ij}\dot{\varepsilon}_{ij}^{EL} + q\dot{\varepsilon}_P + \tau_i\dot{\varepsilon}_{P,i}\right]dV = \int_S [T_i\dot{u}_i + t\dot{\varepsilon}_P]dS \tag{51}$$

thereby defining work-conjugate stress quantities σ_{ij}, q and τ_i in the domain V occupied by the solid, and the surface tractions T_i and t on the external boundary S of the solid. Balance laws for the stress quantities follow directly from the principle of virtual work:

$$\sigma_{ij,j} = 0 \quad \text{and} \quad q - \tau_{i,i} = \sigma'_{ij}m_{ij} \quad \text{in } V, \tag{52}$$

$$\sigma_{ij}n_j = T_i \quad \text{and} \quad \tau_i n_i = t \quad \text{on } S \tag{53}$$

and $\sigma_{ij} = \sigma_{ji}$.

The inelastic behaviour can be characterised in terms of four-dimensional stress and strain-rate vectors

$$\mathscr{S}_I = \left(q,\ \ell^{-1}\tau_i\right), \quad \dot{\mathscr{E}}_I = \left(\dot{\varepsilon}_P, \ell\dot{\varepsilon}_{P,i}\right), \quad I = 1, \ldots, 4 \tag{54}$$

and their magnitudes

$$\Sigma^2 = \mathscr{S}_I\mathscr{S}_I = q^2 + \ell^{-2}\tau_i\tau_i, \quad \dot{E}_P^2 = \dot{\mathscr{E}}_I\dot{\mathscr{E}}_I = \dot{\varepsilon}_P^2 + \ell^2\dot{\varepsilon}_{P,i}\dot{\varepsilon}_{P,i}. \tag{55}$$

Constitutive laws relating S_I and $\dot{\mathscr{E}}_I$ for elasto-plastic and elasto-viscoplastic solids duplicate those given in Section 3. The constraint (50) reduces the dimension of the relevant vectors from 20 to 4, simplifying the analysis considerably.

The incremental problem can be cast in the form of two kinematical minimum principles analogous to those given in Section 3, see [8]. In the case of elasto-viscoplastic solids, minimum principle I states that, given the current state of stress σ_{ij} and of plastic deformation (ε_P,E_P) everywhere in V, the actual distribution of plastic strain rate $\dot{\varepsilon}_P$ satisfies the minimum statement

Please cite this article in press as: M.I. Idiart et al., Size effects in the bending of thin foils, Int. J. Eng. Sci. (2009), doi:10.1016/j.ijengsci.2009.06.002

$$\int_{S_U} t\dot{\varepsilon}_P^0\, dS = \min_{\dot{\varepsilon}_P}\left\{\int_V \left[\phi(\dot{E}_P) - \sigma'_{ij} m_{ij}\dot{\varepsilon}_P\right] dV - \int_{S_T} t^0\dot{\varepsilon}_P\, dS\right\}, \tag{56}$$

where $\dot{\varepsilon}_P^0$ and t^0 are the prescribed plastic strain rate and higher-order traction, respectively, and the minimum is taken over fields $\dot{\varepsilon}_P \geqslant 0$ such that $\dot{\varepsilon}_P = \dot{\varepsilon}_P^0$ on S_U. The velocity field $\dot{u}_i$ then follows from minimum principle II, which is of the same form as (15) but with $\dot{\varepsilon}_{ij}^{PL}$ given by (50).

6.1. Analysis of elasto-viscoplastic foils

The scalar framework described above is used herein to analyse elasto-viscoplastic foils. The analysis is similar to that outlined in Section 4, except that the plastic strain rate tensor is now

$$\dot{\varepsilon}_{11}^{PL} = -\dot{\varepsilon}_{22}^{PL} = \dot{\varepsilon}_P m_{11}, \quad \dot{\varepsilon}_{12}^{PL} = 0, \quad \dot{\varepsilon}_{i3}^{PL} = 0 \tag{57}$$

the effective plastic strain rate is $\dot{E}_P = \sqrt{\dot{\varepsilon}_P^2 + (\ell\dot{\varepsilon}'_P)^2}$, and the bending moment is given by the first term in (21). The plastic strain rate distribution $\dot{\varepsilon}_P(x_2)$ is obtained by means of minimum principle (56). Due to the symmetry of the problem, the analysis can be again restricted to the upper half of the foil. However, unlike the (odd) function $\dot{\varepsilon}_P(x_2)$ introduced in Section 4, $\dot{\varepsilon}_P$ is non-negative, and so symmetry demands $\dot{\varepsilon}_P(x_2)$ to be an even function. The required boundary condition on the neutral axis is thus $\tau_2(0) = 0$, and minimum principle I takes the form

$$I = \min_{\dot{\varepsilon}_P}\int_0^H \left[\frac{\sigma_0\dot{\varepsilon}_0}{1+m}\left(\frac{\dot{E}_P}{\dot{\varepsilon}_0}\right)^{1+m} - \sigma_{11} m_{11}\dot{\varepsilon}_P\right] dx_2, \tag{58}$$

where the minimum is taken over fields $\dot{\varepsilon}_P \geqslant 0$. Numerical minimization and time integration are carried out following a similar strategy to that outlined in Appendix A. It should be noted, however, that stress states with vanishing deviatoric Cauchy stress require special treatment. When $\sigma'_{ij} = 0$, the tensor m_{ij} defined by $(50)_2$ becomes a set-valued function. In classical (visco-)plasticity this poses no problem, as the plastic constitutive law demands $\dot{\varepsilon}_P = 0$, and therefore $\dot{\varepsilon}_{ij}^{PL} = 0$. In strain gradient plasticity, it is possible to have a domain where $\dot{\varepsilon}_P > 0$ yet $\sigma'_{ij} = 0$. To handle this case numerically, we introduce the regularization

$$m_{ij} = \begin{cases} \frac{3}{2}\frac{\sigma'_{ij}}{\sigma_e}, & \text{if } \sigma_e \geqslant \sigma_c, \\ \frac{3}{2}\frac{\sigma'_{ij}}{\sigma_c}, & \text{otherwise}, \end{cases} \tag{59}$$

where σ_c is a small stress threshold relative to σ_0. Results were found to be insensitive to the choice of σ_c; the numerical results given below correspond to the choice $\sigma_c = 0.01\sigma_0$.

Predictions derived with the above 'scalar' theory are confronted in Fig. 4 with the 'tensorial' predictions of Section 4. A weaker size effect on bending response is predicted by the scalar theory: thin foils with thickness ratio $\ell/H = 1$ are ~ 1.7 times stronger in bending than thick foils ($\ell/H = 0$); recall that the tensorial theory gave a strength elevation of ~ 2.5, see Fig. 4a. The distribution of Cauchy stress $\sigma_{11}(x_2)$ at $2H\kappa/\sqrt{3} = 0.05$ for the scalar theory is included in Figs. 4d and 5b. The distribution is markedly different from that given by the tensorial theory. It is characterised by the feature that $\sigma_e \leqslant \sigma_c$ and $0 \leqslant m_{11} \leqslant (\sqrt{3}/2)$ over a central domain of size $\sim 0.8\ell$, and on the neutral axis $\dot{\varepsilon}_{11}^{PL}$ and m_{11} both go to zero while $\dot{\varepsilon}_P$ remains finite, see Fig. 4b and e. Finally, the distributions of (q/σ_0) and $(\tau_2/\ell\sigma_0)$ are shown in Fig. 4c and f. It is evident from these figures that flow is activated mainly by the stress quantity q. This is in contrast to the tensorial predictions, where flow was found to be mainly activated by the higher-order stresses $\ell^{-1}\tau_{112}$. We emphasise, however, that the scalar and tensorial versions of the strain gradient theory both reduce to classical J_2 flow theory in the limit $\ell/H \to 0$.

7. Application to metallic foams

The above developments for the tensorial version of the strain gradient theory can be used immediately to predict the effect of cell size on the yield strength σ_f of an open-cell metallic foam. Recall that $\sigma_f \propto M/(2L)^3$, where M is the fully plastic moment of the cell ligaments of length $2L$ (see [12]). The elevation in macroscopic strength thus equals the elevation in collapse moment of the ligaments, which can be approximated by (33) and (34). Recalling that the relative density of these foams depends upon the average thickness-to-length ratio H/L of the ligaments according to $\bar{\rho} = C_\rho(H/L)^2$, we can write

$$\frac{\sigma_f}{\sigma_0} = C_f f_y(\beta)\bar{\rho}^{3/2}, \quad \beta = \frac{\ell}{L}\left(\frac{C_\rho}{\bar{\rho}}\right)^{1/2}, \tag{60}$$

where the proportionality constants are in the ranges $C_\rho = 1.06 - 4.61$ and $C_f = 0.1 - 1$ [12]. The exponent 3/2 reflects the fact that the ligaments bend under the macroscopic loading. Consider the typical case of $\bar{\rho} = 0.05$ and $C_\rho = 1.1$; we anticipate from (60) that the uniaxial strength of the foam is doubled when $2L < 10\ell \approx 50\ \mu\text{m}$, assuming $\ell = 5\ \mu\text{m}$ for example.

A similar conclusion can be drawn for a prismatic foam such as a regular hexagonal honeycomb. For this 2D lattice, the in-plane compressive strength $\sigma_f \propto M/(2L)^2$, and the relative density is $\bar{\rho} = (2/\sqrt{3})(H/L)$ [12]. In view of (33) and (34) we can thus write

Please cite this article in press as: M.I. Idiart et al., Size effects in the bending of thin foils, Int. J. Eng. Sci. (2009), doi:10.1016/j.ijengsci.2009.06.002

$$\frac{\sigma_f}{\sigma_0} = C_f' f_y(\beta)\bar{\rho}^2, \quad \beta = \frac{2\ell}{\sqrt{3}L}\frac{1}{\bar{\rho}}. \tag{61}$$

For the case of $\bar{\rho} = 0.05$, the uniaxial strength is doubled for $2L < 50\ell \approx 250\ \mu\text{m}$, for the choice $\ell = 5\ \mu\text{m}$.

These values of cell size are well below the practical range for conventional metallic lattices: cell sizes usually exceed 1 mm. However, microlattices do exist on a sub-millimeter length scale, made by lithography for example. For such materials, size effects are anticipated.

Acknowledgements

This research is based upon work supported by the Engineering and Physical Sciences Research Council (EPSRC), UK, through a Materials Modelling Programme, and by the European Community through the Sixth Framework Programme Integrated Project IP 026467-2 MANUDIRECT.

Appendix A. Numerical solution of elasto-plastic problem

A.1. Spatial minimization

The functional (23) is discretised into N_e linear elements of equal length $L = H/N_e$, and minimized with respect to the nodal amplitudes of plastic strain rate $\hat{\varepsilon}_P^{(i)}$ $(i = 1, \ldots, N_e + 1)$. The integrand in (23) is evaluated at the element mid-points $x_m^{(i)}$, so that the discretised integral reads

$$I = L\sum_{i=1}^{N_e}\left[\sigma_y(E_P^{(i)})\widehat{E}_P^{(i)} - \frac{\sqrt{3}}{2}\sigma_{11}^{(i)}\hat{\varepsilon}_m^{(i)}\right], \tag{62}$$

where

$$\hat{\varepsilon}_m^{(i)} = \frac{\hat{\varepsilon}_P^{(i+1)} + \hat{\varepsilon}_P^{(i)}}{2}, \quad \hat{\varepsilon}_d^{(i)} = \ell\frac{\hat{\varepsilon}_P^{(i+1)} - \hat{\varepsilon}_P^{(i)}}{L}, \quad \widehat{E}_P^{(i)} = \sqrt{(\hat{\varepsilon}_m^{(i)})^2 + (\hat{\varepsilon}_d^{(i)})^2} \tag{63}$$

and $\sigma_{11}^{(i)}, E_P^{(i)}$ are given quantities (see below). The nodal amplitudes are constrained by $\hat{\varepsilon}_P^{(1)} = 0$ and $\sum_{i=1}^{N_e}(\hat{\varepsilon}_m^{(i)})^2 = H/L$. The discretised functional (62) is a non-smooth function of the nodal amplitudes. Thus, even though its minimum value is attained at a stationary point, a numerical algorithm suitable for non-smooth optimization is required. We employ a direct search complex algorithm implemented as subroutine *BCPOL* in the commercial Fortran Library IMSL.[3]

A.2. Time integration

An explicit forward-Euler scheme with fixed step $\Delta\kappa$ is used to integrate the incremental solution up in time. At the $k+1$ step we proceed as follows:

(i) Given the curvature and plastic state $(\kappa_k, \varepsilon_{P;k}^{(i)}, E_{P;k}^{(i)})$ at time step k, compute the nodal plastic strain rates $\hat{\varepsilon}_P^{(i)}$ by minimizing (62). The elasticity relation (19) provides

$$\sigma_{11;k}^{(i)} = \frac{4}{3}E\left(\kappa_k x_m^{(i)} - \frac{\sqrt{3}}{2}\frac{\varepsilon_{P;k}^{(i+1)} + \varepsilon_{P;k}^{(i)}}{2}\right). \tag{64}$$

(ii) Compute the ratio $(\dot{\lambda}/\dot{\kappa})$ from discretised version of (25),

$$\frac{\dot{\lambda}}{\dot{\kappa}} = \frac{2}{\sqrt{3}}E\frac{\sum_{i=1}^{N_e} x_m^{(i)}\hat{\varepsilon}_m^{(i)}}{\sum_{i=1}^{N_e}\left[E\hat{\varepsilon}_m^{(i)^2} + h(E_{P;k}^{(i)})\widehat{E}_P^{(i)^2}\right]}. \tag{65}$$

(iii) Update curvature and plastic state,

$$\kappa_{k+1} = \kappa_k + \Delta\kappa, \tag{66}$$

$$\varepsilon_{P;k+1}^{(i)} = \varepsilon_{P;k}^{(i)} + (\dot{\lambda}/\dot{\kappa})\hat{\varepsilon}_P^{(i)}\,\Delta\kappa, \quad i = 1, \ldots, N_e + 1, \tag{67}$$

$$E_{P;k+1}^{(i)} = E_{P;k}^{(i)} + (\dot{\lambda}/\dot{\kappa})\widehat{E}_P^{(i)}\,\Delta\kappa, \quad i = 1, \ldots, N_e. \tag{68}$$

(iv) Compute moment M_{k+1} from discretised version of (21),

$$M_{k+1} = 2L\sum_{i=1}^{N_e} x_m^{(i)}\sigma_{11;k+1}^{(i)}. \tag{69}$$

[3] IMSL Fortran Library 3.0, Visual Numerics, Inc., Houston, TX, USA.

Please cite this article in press as: M.I. Idiart et al., Size effects in the bending of thin foils, Int. J. Eng. Sci. (2009), doi:10.1016/j.ijengsci.2009.06.002

The Ramberg–Osgood law (22) exhibits infinite hardening rate at zero plastic strain, and so the above scheme cannot be applied at the first time step. An implicit backward-Euler scheme is used there instead: relations (67) are treated as a system of nonlinear equations for the nodal plastic strains $\varepsilon_{P;1}^{(i)}$, where the $\hat{\varepsilon}_P^{(i)}$ are obtained from (62) evaluated at the unknown $\varepsilon_{P;1}^{(i)}$, and the equations are solved by a fixed-point method.

References

[1] L. Anand, M.E. Gurtin, S.P. Lele, C. Gething, A one-dimensional theory of strain-gradient plasticity: formulation, analysis, numerical results, J. Mech. Phys. Solids 53 (2005) 1789–1826.
[2] V.S. Deshpande, A. Needleman, E. Van der Giessen, Finite strain discrete dislocation plasticity, J. Mech. Phys. Solids 51 (2003) 2057–2083.
[3] B. Ehrler, X.D. Hou, T.T. Zhu, K.M.Y. P'ng, C.J. Walker, A.J. Bushby, D.J. Dunstan, Grain size and sample size interact to determine strength in a soft metal, Philos. Mag. 88 (2008) 3043–3050.
[4] R.A.B. Engelen, N.A. Fleck, R.H.J. Peerlings, M.G.D. Geers, An evaluation of higher-order plasticity theories for predicting size effects and localisation, Int. J. Solids Struct. 43 (2006) 1857–1877.
[5] A.G. Evans, J.W. Hutchinson, A critical assessment of theories of strain gradient plasticity, Acta Mater. 57 (2009) 1675–1688.
[6] N.A. Fleck, J.W. Hutchinson, Strain gradient plasticity, Adv. Appl. Mech. 33 (1997) 295–361.
[7] N.A. Fleck, J.W. Hutchinson, A reformulation of strain gradient plasticity, J. Mech. Phys. Solids 49 (2001) 2245–2271.
[8] N.A. Fleck, J.R. Willis, A mathematical basis for strain gradient plasticity theory. Part I: scalar plastic multiplier, J. Mech. Phys. Solids 57 (2009) 161–177.
[9] N.A. Fleck, J.R. Willis, A mathematical basis for strain gradient plasticity theory. Part II: tensorial plastic multiplier, J. Mech. Phys. Solids 57 (2009) 1045–1057.
[10] N.A. Fleck, G.M. Muller, M.F. Ashby, J.W. Hutchinson, Strain gradient plasticity: theory and experiment, Acta Metall. Mater. 42 (1994) 475–487.
[11] P. Fredriksson, P. Gudmundson, Size-dependent yield strength of thin films, Int. J. Plast. 21 (2005) 1834–1854.
[12] L.J. Gibson, M.F. Ashby, Cellular Solids: Structure and Properties, second ed., Cambridge University Press, 1997.
[13] P. Gudmundson, A unified treatment of strain gradient plasticity, J. Mech. Phys. Solids 52 (2004) 1379–1406.
[14] M.E. Gurtin, On the plasticity of single crystals: free energy, microforces, plastic-strain gradients, J. Mech. Phys. Solids 48 (2000) 989–1036.
[15] R. Hill, On the state of stress in a plastic-rigid body at the yield point, Philos. Mag. 42 (1951) 868–875.
[16] J.W. Hutchinson, Plasticity at the micron scale, Int. J. Solids Struct. 37 (2000) 225–238.
[17] J.W. Hutchinson, A.G. Evans, Mechanics of materials: top-down approaches to fracture, Acta Mater. 48 (2000) 125–135.
[18] J.B. Martin, On the kinematic minimum principle for the rate problem in classical plasticity, J. Mech. Phys. Solids 23 (1975) 123–128.
[19] P. Moreau, M. Raulic, K.M.Y. P'ng, G. Gannaway, P. Anderson, W.P. Gillin, A.J. Bushby, D.J. Dunstan, Measurement of the size effect in the yield strength of nickel foils, Philos. Mag. Lett. 85 (2005) 339–343.
[20] C. Motz, T. Schöberl, R. Pippan, Mechanical properties of micro-sized copper bending beams machined by the focused ion beam technique, Acta Mater. 53 (2005) 4269–4279.
[21] C.F. Niordson, On higher-order boundary conditions at elasticplastic boundaries in strain-gradient plasticity, Philos. Mag. 88 (2008) 3731–3745.
[22] R. Sedláček, Bending of thin crystalline strips: comparison of continuum dislocation-based models, Mater. Sci. Eng. A 400–401 (2005) 439–442.
[23] P. Shrotriya, S.M. Allameh, J. Lou, T. Buchheit, W.O. Soboyejo, On the measurement of the plasticity length scale parameter in LIGA nickel foils, Mech. Mater. 35 (2003) 233–243.
[24] J.S. Stölken, A.G. Evans, A microbend test method for measuring the plasticity length scale, Acta Mater. 46 (1998) 5109–5115.
[25] N.S. Weingarten, R.L.B. Selinger, Size effects and dislocation patterning in two-dimensional bending, J. Mech. Phys. Solids 55 (2007) 1182–1195.
[26] S. Yefimov, E. Van der Giessen, I. Groma, Bending of a single crystal: discrete dislocation and nonlocal crystal plasticity simulations, Modell. Simul. Mater. Sci. Eng. 12 (2004) 1069–1086.
[27] M. Zaiser, N. Nikitas, T. Hochrainer, E.C. Aifantis, Modelling size effects using 3D density-based dislocation dynamics, Philos. Mag. 87 (2007) 1283–1306.

Please cite this article in press as: M.I. Idiart et al., Size effects in the bending of thin foils, Int. J. Eng. Sci. (2009), doi:10.1016/j.ijengsci.2009.06.002